Critical Factors for Detection of Biphasic Changes in Membrane Properties at Specific Sterol Mole Fractions for Maximal Superlattice Formation

Berenice Venegas,[†] István P. Sugár,[‡] and Parkson Lee-Gau Chong*[,†]

Department of Biochemistry, Temple University School of Medicine, 3420 N. Broad St, Philadelphia, Pennsylvania 19140 and Graduate School of Biological Sciences, Mount Sinai Medical Center, One Gustave Levy Place, New York, New York 10029

Received: January 10, 2007; In Final Form: February 27, 2007

Here we use the excitation generalized polarization (GP_{ex}) of 6-lauroyl-2-(dimethylamino)naphthalene (Laurdan) fluorescence in fluid cholesterol/1-palmitoyl-2-oleoyl-L-α-phosphatidylcholine large unilamellar vesicles to explore the experimental conditions that would be required in order to detect a biphasic change in membrane properties at specific sterol mole fractions (C_r) (e.g., 20.0, 22.2, 25.0, 33.3, 40.0, and 50.0 mol %) for maximal sterol superlattice formation. Laurdan's GP_{ex} changes with sterol content in an alternating manner, showing minima (termed as GP_{ex} dips) at $\sim C_r$. GP_{ex} dips are detectable if the vesicles are preincubated for a sufficient time period and protected from sterol oxidation. In most cases, vesicles with a higher lipid concentration take a longer time to show a GP_{ex} dip at C_r. The depth of the GP_{ex} dip increases with increasing incubation time and eventually reaches a plateau, at which the maximum area covered by superlattices is expected to be achieved. However, if the vesicles are not protected against sterol oxidation, the GP_{ex} dips are attenuated or obliterated. These effects can be attributed to the increased inter-bilayer lipid exchange and the increased vesicle−vesicle interactions present at high lipid (vesicle) concentrations as well as the decreased interactions between oxysterols and phospholipids. These possible explanations have been incorporated into a kinetic model that is able to calculate the effects of sterol oxidation and lipid concentration on the depth of the GP_{ex} dip. The depth of the GP_{ex} dip, the required incubation time for the dip formation, and the lipid concentration dependence of the GP_{ex} dip vary with C_r, suggesting different physical properties for different sterol superlattices. To detect a biphasic change in membrane properties at C_r, one should also use small sterol mole fraction increments over a wide range, keep all of the vesicles in the same sample set under the same thermal history, and consider lipid concentration, probe type, and C_r value. These results improve our mechanistic understanding of sterol superlattice formation and explain why some studies, especially those requiring high lipid concentrations, did not detect a biphasic change in membrane properties at C_r.

Introduction

The functions of lipid rafts-associated proteins are sensitive to cell cholesterol content (for example, see ref 1 and 2). However, the molecular basis of the high cholesterol sensitivity is poorly understood. One of the fundamental questions needed to be addressed is how cholesterol content affects membrane lateral organization, which can be an important determinant of membrane functions. Lipid microdomains in cells observed by microscopy techniques[3−6] may be related to the functional rafts[7,8] implicated in cell biology studies. Variations in cholesterol content do change the size and shape of the visualized microdomains. However, to date, the molecular lateral organization of cholesterol inside and outside those microdomains is not known, rendering it difficult to fully understand the effect of cholesterol content on cellular functions of lipid rafts-associated proteins.

To reveal the physical principles underlying the effect of cholesterol content on membrane lateral organization, the use of well-defined model membranes is a necessity. Previous studies have suggested that cholesterol can be regularly distributed in lipid membranes. This sterol regular distribution (e.g., sterol superlattice) model (Figure 1;[9] reviewed in ref 10−12) proposes that sterols (e.g., cholesterol, ergosterol, and dehydroergosterol) can be organized in a regular lattice within the matrix lattice formed by membrane lipid acyl chains and sterol molecules. Regularly distributed sterol superlattices (shaded areas, Figure 1) and irregularly distributed lipid areas (blank areas, Figure 1) always coexist in fluid sterol-containing membranes (rectangle-like objects, Figure 1), with the ratio of irregular to regular regions (R; solid line in the bottom diagram of Figure 1) reaching a local minimum at critical sterol mole fractions (C_r) (e.g., 20.0, 22.2, 25.0, 33.3, 40.0, and 50.0 mol % sterol). The C_r values can be calculated from the superlattice theories.[9,13−17] In the regular regions, sterol molecules (dark circles, Figure 1) are distributed into either hexagonal or centered rectangular superlattices. Membrane defects or membrane free volume (V; solid line in the bottom diagram of Figure 1) varies with sterol content in an alternating manner, exhibiting a local minimum at C_r (Figure 1). The shape and size of the regular distribution fluctuate with time, and lipids inside and outside the regular regions undergo constant exchanges. The thermal fluctuations result in small un-ordered inner islands in the large regular regions which can be considered as the inner periphery of the regular regions. The perimeter, outer plus inner, is

* To whom correspondence should be addressed. Tel.: 215-707-4182. Fax: 215-707-7536. E-mail: pchong02@temple.edu.
[†] Temple University School of Medicine.
[‡] Mount Sinai Medical Center.

10.1021/jp070222k CCC: $37.00
Published on Web 04/19/2007

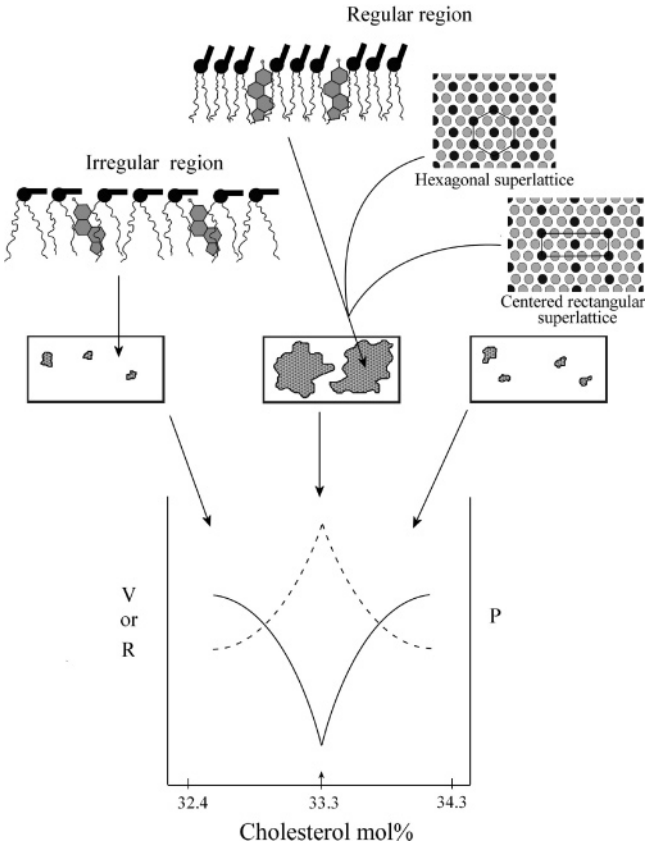

Figure 1. Schematic diagram showing the current concepts underlying the sterol regular distribution model. The rectangle-like objects represent a lipid membrane, where regular (shaded areas) and irregular (blank areas) regions coexist. In regular regions, sterol molecules are regularly distributed into either hexagonal or centered rectangular superlattices within the host lipid matrix. There is a biphasic change in proportion of irregular region to regular region (*R*, solid line), membrane free volume (*V*, solid line), and the perimeter of regular region (*P*, dashed line) with membrane cholesterol content in the neighborhood of a critical sterol mole fraction C_r (e.g., 33.3 mol % cholesterol as indicated by arrow) theoretically predicted for maximal superlattice formation.

proportional to the size of the regular region. Thus, the perimeter (*P*; dashed line in the bottom diagram of Figure 1) of the regular regions may increase abruptly at C_r causing a large increase in the interfacial area between the regular and irregular regions, making sterols at C_r more exposed to the aqueous phase than sterols at non-C_r.

Sterol regular distributions have been simulated by the Monte Carlo method.[18−20] The simulations also revealed the driving forces for superlattice formation. First, there is a large, favorable cholesterol−phospholipid attraction. Second, cholesterol has a condensing effect on neighboring acyl chains by reducing the number of gauche configurations, causing an unfavorable entropy loss. The fine balance between the unfavorable entropy loss through the multibody interactions of cholesterol with nearest neighbors and the overall favorable hydrophobic effect drives the sterol molecules to form superlattice-like regular distributions.[20]

The experimental evidence for sterol superlattice formation in liposomes mainly came from the detection of multiple biphasic changes in membrane properties at C_r (reviewed in ref 10). For example, the partitioning of the antifungal drug nystatin into liposomes has been shown to vary with membrane sterol content in an alternating manner, showing minimal partitioning at C_r.[21,22] The activities of surface acting enzymes phospholipase A2 (PLA2) and cholesterol oxidase (COD) also vary with sterol content in an alternating manner.[22,23] PLA2 exhibits an activity minimum at C_r, whereas COD displays an activity maximum at C_r, all in agreement with the sterol regular distribution model and consistent with the special substrate requirements of these two enzymes (discussed in ref 22). The initial rate of sterol oxidation induced by free radicals has also been found to change with sterol content in an alternating manner, exhibiting a local maximum at C_r.[24] This result agrees with the sterol regular distribution model in that sterols at C_r are more exposed to the aqueous phase, where the free radicals reside, than those at non-C_r.

However, to detect the multiple biphasic changes at C_r is not a trivial matter. Our previous studies[9,11,13,25] indicated that, for this detection, the sterol mole fractions must be varied with small increments over a wide range, the lipids must be mixed thoroughly in organic solvent before vesicle formation, and vesicles must be subject to cooling and heating cycles and sufficient incubation. In addition, all of the vesicles in the same sample set should be examined under the same thermal history, and the sterol mole fraction in each vesicle sample must be determined highly accurately.

In the present study, we have used excitation generalized polarization (GP_{ex}) of 6-lauroyl-2-(dimethylamino)naphthalene (Laurdan) fluorescence in fluid cholesterol/1-palmitoyl-2-oleoyl-L-α-phosphatidylcholine (POPC) large unilamellar vesicles (LUVs) to further explore the experimental conditions that would be required in order to detect multiple biphasic changes at the predicted C_r values. Our data showed that Laurdan's GP_{ex} changes with sterol content in an alternating manner, displaying minima (termed GP_{ex} dips) at C_r and that sterol oxidation and lipid (or vesicle) concentration can greatly affect the detection of the biphasic changes in Laurdan's GP_{ex} at C_r. Liposome samples with a higher lipid concentration take a longer time to show a GP_{ex} dip at C_r. The extent of the biphasic change and the required incubation time vary with C_r, suggesting different physical properties (e.g., lattice constant and interaction energy) for different sterol superlattices. These results help to standardize the method to detect multiple biphasic changes in membrane properties at C_r, gain a mechanistic understanding of sterol superlattice formation, and explain why some studies, especially those requiring high lipid concentrations, did not detect biphasic changes at C_r. The physical principles revealed in this study may eventually help to understand the effects of cholesterol on lipid rafts and the rafts-associated cell functions.

Materials and Methods

Materials. Appropriate amounts of POPC and cholesterol (Avanti Polar Lipids, Alabaster, AL) were dissolved in chloroform to make stock solutions (stored at −20 °C). The amount of cholesterol in the stock solution was determined using a cholesterol reagent (Cholesterol E) obtained from Wako Chemicals (Richmond, VA). The concentrations of POPC in the stock solution and in vesicles were determined by the method of Bartlett.[26] The stock solutions of Laurdan and 1,6-diphenyl-1,3,5-hexatriene (DPH) (Invitrogen-Molecular Probes, Eugene, OR; 40 μM) were made in dimethylsulfoxide (DMSO) and stored in the dark at 4 °C.

Preparation of Large Unilamellar Vesicles (LUV). Appropriate amounts of POPC and cholesterol in stock solutions were pipetted into tubes and dried under N_2 until there was no visible solvent; lipids were then further dried overnight under high vacuum. The dried lipids were reconstituted with 50 mM Tris buffer (pH 7.2) containing 0.02% NaN_3 and 10 mM EDTA at 40 °C, flushed with N_2, sealed, and vortexed for 3 min at

40 °C to form multilamellar vesicles (MLVs). The MLVs were cooled to 4 °C for 30 min and then incubated at 40 °C for 30 min. This cooling−heating cycle was repeated two more times to ensure an even distribution of lipids within each monolayer of the vesicles. MLVs were then incubated under argon at room temperature for 4 days. LUVs were made from MLVs by passing the vesicles 10 times through two stacked 200-nm Nucleopore polycarbonate membranes under N_2 gas pressure using an extruder (Lipex Biomembranes, Vancouver, Canada). The LUV samples were flushed with argon, sealed, and stored in a desiccator chamber under vacuum at room temperature for the desired incubation period prior to Laurdan GP_{ex} or DPH polarization measurements. During this incubation time, argon in the sample tubes was replenished two to three times a week. These procedures are critical in protecting cholesterol from autooxidation during vesicle incubation. Before fluorescence readings, phospholipid concentration was measured again to determine the amount of vesicles needed to be pipetted into the fluorescence cuvette for the measurements.

A typical sample set spanned a predicted C_r. Every sample within the set contained the same amount of cholesterol but varied only in the sterol mole percent. This was accomplished by varying the number of moles of POPC per sample, while leaving the number of moles of cholesterol constant. Typically, the sterol mole percent was increased by ∼0.3−0.4 mol % for each sample. The sterol mole percents in vesicles before and after extrusion differ little (≤0.2 mol %).[22] Thus, for convenience, the sterol mole percents in MLVs were used to assess the relationship between sterol content and Laurdan's GP_{ex} (or DPH polarization) in LUVs. Within a sample set, one or two sample triplicates were made to obtain typical standard deviations. Vesicle size was measured by photon correlation spectroscopy using a Malvern Zetasizer HS-1000 spectrometer (Worcs, UK; light source: 10 mW He−Ne laser at 633 nm).

Stock Samples, Testing Samples, and Reading Samples. Figure 2 depicts the experimental design used in this study. A stock sample set (for the general definition of a sample set, see the preceding paragraph) was prepared for each C_r examined. The C_r values examined were 20.0, 22.2, 25.0, 33.3, 40.0, and 50.0 mol % cholesterol. The concentration of POPC in each sample of the same stock sample set was ∼5 mM. The stock samples were then diluted to make different sets of testing samples at different POPC concentrations ranging from 40 to 800 μM (Figure 2). In this way, all of the testing samples had virtually the same thermal history and similar vesicle size and size distribution; the only significant difference was the number of vesicles in each testing sample set. The testing samples were used to test the experimental conditions (e.g., vesicle incubation time at different POPC concentrations) that would be required in order to detect multiple biphasic changes in Laurdan's GP_{ex} or DPH fluorescence polarization at C_r. The reading samples were diluted from the testing samples at ∼1 h before fluorescence measurements; the concentration of POPC in all of the reading samples was kept at 22.2 μM.

Measurements of Laurdan's GP_{ex} and DPH Fluorescence Polarization. Laurdan is an environmentally sensitive fluorescent probe with its chromophore located near the phospholipid polar headgroup region.[27,28] For fluorescence labeling, 5 μL of 40 μM Laurdan in DMSO was added to the reading samples, which contained 40 nmol POPC in a final volume of 1.8 mL (i.e., 22.2 μM POPC). This yielded a probe-to-POPC ratio of 1/200. The amount of DMSO added has previously been shown not to perturb the membrane structure to any significant extent.[29,30] After the vesicles in the reading samples were labeled with Laurdan at 24 °C for 1 h, the emission spectra of Laurdan fluorescence were measured under gentle stirring at 24 °C on an ISS K2 fluorometer (Champaign, IL). The background readings from vesicles without the probe were subtracted from the sample readings. The excitation generalized polarization ($GP_{ex} = (I_{435} - I_{500})/(I_{435} + I_{500})$)[27,31] was then calculated from the spectral readings. Here I_{435} and I_{500} are the fluorescence intensities at 435 and 500 nm, respectively. The sample was excited at 340 nm. All reading samples had an absorbance of ∼0.06 at 340 nm. Using a similar fluorescence labeling procedure, the steady-state polarization of DPH fluorescence in cholesterol/POPC LUVs was measured through a KV-408 filter with $\lambda_{ex} = 350$ nm on the ISS K2 fluorometer. Note that Laurdan and DPH were not present in the testing or stock samples; these probes were introduced only to the reading samples 1 h prior to the fluorescence measurements.

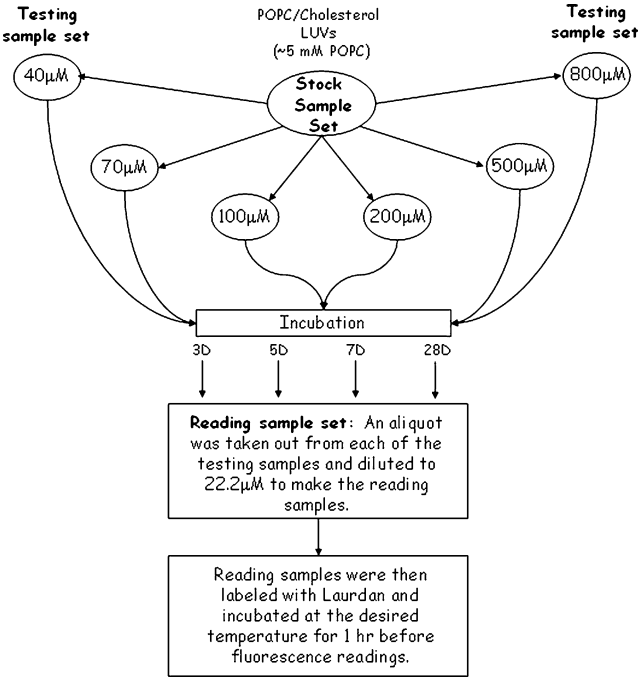

Figure 2. Outlines of the experimental designs for the determination of the effects of incubation time and lipid concentration on Laurdan's GP_{ex} in vesicles. The testing sample sets at various lipid concentrations (as indicated) were prepared from the same stock sample set. The vesicle incubation time of a given testing sample set varied typically from 3 days to 28 days. During vesicle incubation, the samples were protected from clolesterol oxidation as described in Materials and Methods unless otherwise specified. The reading samples were prepared from the testing samples by dilution to 22.2 μM POPC. Specifically, 5 μL of 40 μM Laurdan in DMSO was added to the reading samples (1.8 mL of 22.2 μM POPC) ∼1 h prior to fluorescence measurements. In this time frame, Laurdan's fluorescence intensity in vesicles reached a steady-state level.

HPLC Analysis of Cholesterol Oxidation. Cholesterol autooxidation in cholesterol/POPC LUVs was checked using high performance liquid chromatography (HPLC; model Breeze, Waters, Milford, MA) with a C18 reversed-phase column (3.9 × 150 mm, 5 μm Symmetry, Waters, Milford, MA). In this experiment, lipids were first extracted from vesicles using 3 volumes of chloroform/methanol (2:1, v/v) with vigorous agitation for 3 min, followed by low-speed centrifugation (∼1000 rpm) for 10 min. The lower phase was taken out and dried by N_2, redissolved in 100 μL of methanol/acetonitrile (2:1, v/v) containing a trace amount of Laurdan (used as an internal standard), and then injected into the HPLC column. The sample

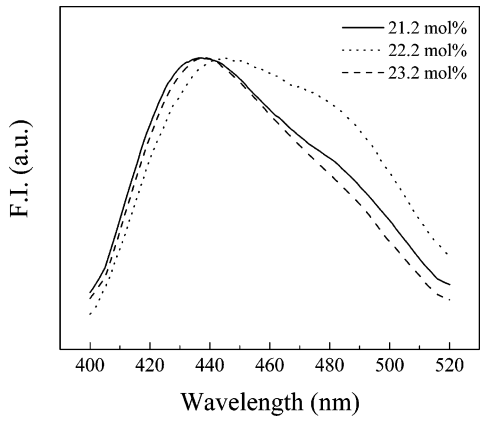

Figure 3. Emission spectra of Laurdan in cholesterol/POPC LUVs at three different cholesterol mole fractions: 21.0, 22.2, and 23.2 mol %. 22.2 mol % is a critical mole fraction (C_r) for centered rectangular superlattices, whereas 21.0 and 23.2 mol % are non-C_r values. [POPC] = 40 μM. Temperature = 24 °C. The LUVs were incubated for 3 days prior to the spectral measurements.

was eluted with methanol/acetonitrile (2:1, v/v) at a flow rate of 1.5 mL/min. The eluted products were detected by absorbance at 240 nm.

Results and Discussion

A. Use of Small Sterol Mole Fraction Increments over a Wide Range. *Multiple GP_{ex} Dips.* Figure 3 shows that there is a distinct difference in Laurdan's emission spectrum between cholesterol/POPC LUVs at the critical sterol mole fraction (C_r) 22.2 mol % and those at the neighboring non-critical sterol mole fractions (non-C_r) (e.g., 21.2 and 23.2 mol %). At 21.2 mol % (a non-C_r), the dominating peak is located at ~436 nm. In contrast, at 22.2 mol % (a C_r) the dominating peak is shifted to ~446 nm in conjunction with an increase in the shoulder area (~480 nm). When the cholesterol mole fraction was further increased to 23.2 mol % (a non-C_r), the emission spectrum was reversed almost completely to that detected at 21.2 mol %. Figure 3 clearly shows a biphasic change in Laurdan's emission spectrum at the C_r value 22.2 mol %. Similar results were obtained from samples in other C_r regions (data not shown). The observation that Laurdan's emission spectrum at C_r is more red-shifted compared to the spectra at neighboring non-C_r indicates that the chromophore of Laurdan is subject to more solvent relaxation, probably due to more exposure to the aqueous phase or lipid polar groups,[31,32] at C_r than at neighboring non-C_r.

The biphasic spectral change at C_r is even more apparent in terms of Laurdan's excitation generalized polarization (GP_{ex}, defined in Materials and Methods).[27,31] The values of GP_{ex} were calculated from Laurdan's emission spectra (e.g., Figure 3) and used as an index of membrane packing near the phospholipid glycerol backbone regions. The plot of GP_{ex} against cholesterol mole percent shows a biphasic change (termed GP_{ex} dip) at 19.7, 22.2, 25.0, 26.2, 33.3, 40.3, and 50.0 mol % cholesterol (Figure 4A). Within the experimental errors (0.1−0.4 mol %),[13] these mole fractions, except for 26.2 mol %, are in excellent agreement with the C_r values (20.0, 22.2, 25.0, 33.3, 40.0, and 50.0 mol %) theoretically predicted for maximal superlattice formation in the mole fraction range examined (18.3−52.4 mol % cholesterol).[10−13] The dip at 26.2 mol % is not predicted by the hexagonal or centered rectangular superlattice theories. However, a biphasic change in membrane properties around this sterol mole fraction (~26.0−26.5 mol %) has been observed in previous studies,[13,23] although their physical origin is not clear.

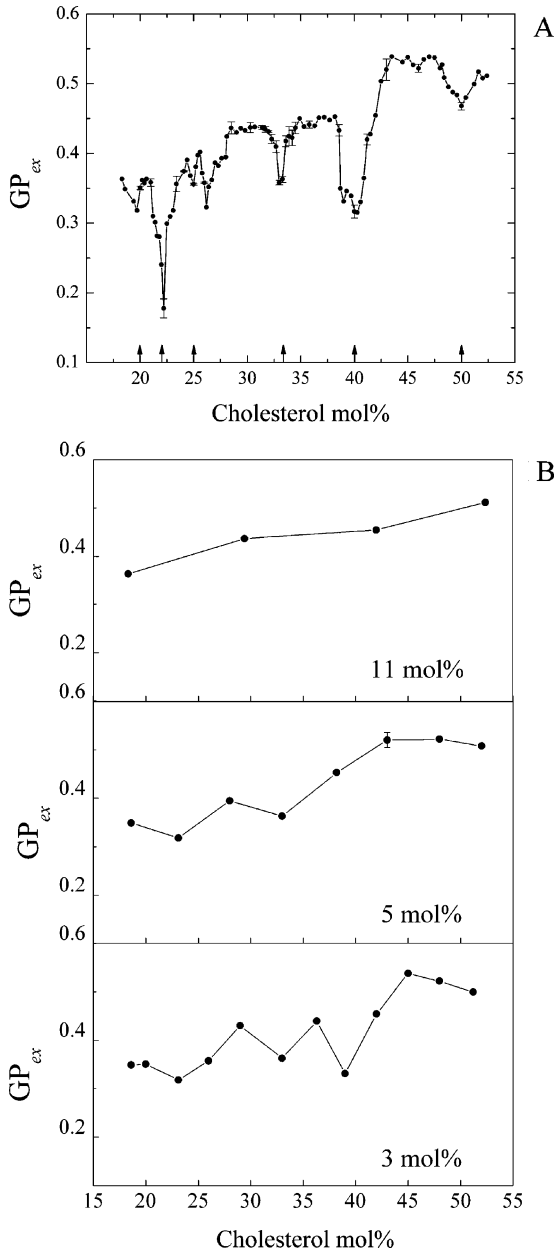

Figure 4. (A) Laurdan's GP_{ex} as a function of cholesterol content in cholesterol/POPC LUV (diameter ~160−180 nm). GP_{ex} was measured at 24 °C. The vertical bars are the standard deviations of GP_{ex} obtained from three independently prepared vesicle samples. [POPC] was 40−60 μM and vesicles were incubated 7 days or more prior to GP_{ex} measurements. Arrows indicate the theoretically predicted critical sterol mole fractions (C_r) for maximal superlattice formation in the mole percent range examined. (B) The data in panel A are replotted using larger sterol mole fraction increments such as 3, 5, or 11 mol % sterol.

The observation that Laurdan becomes more accessible to the aqueous phase at C_r than at non-C_r can be understood in terms of relocation of Laurdan molecules in accordance with the lateral organization variations with cholesterol content depicted in Figure 1. Previous infrared studies showed that the chromophore of Laurdan causes significant local membrane perturbations.[28] These perturbations would attenuate or abolish sterol superlattice formation, which requires stringent geometric arrangements with no tolerance of defects in the bilayer region. Thus, it is likely that Laurdan molecules are excluded from the regularly distributed sterol superlattice regions. This idea is supported by the recent microscopy observation of nonfluorescent regions in giant unilamellar vesicles labeled with Laur-

dan.[32,33] The lipids in those nonfluorescent regions were believed to be tightly packed.[32,33] This concept is also in agreement with a recent finding that nystatin channels are located at the boundaries, not the interiors, of lipid superlattices.[34] Membrane defects are allowed to exist in the irregular regions[16] and could be even more abundant in the interfaces between regular and irregular regions. Laurdan with a bulky naphthalene ring may partition favorably to membrane areas with more defects.[28] As such, the interfacial regions are likely to be the major sites for Laurdan, whereas the irregular regions could also accommodate this probe. At C_r, the regular regions and the total perimeter (P) of the regular regions (i.e., the amount of the interfacial regions) reach a local maximum, according to the sterol regular distribution model (Figure 1).[21,22] This situation would force more Laurdan molecules to relocate to the interfacial regions. Since these regions contain membrane defects where water penetrates more easily and since GP_{ex} decreases with increasing water content,[35] the overall GP_{ex} exhibits a local minimum at C_r (Figure 4A). In this way, the GP_{ex} dips observed at C_r (Figure 4A) can be explained by the concepts proposed in the sterol regular distribution model.

Another possible explanation for the appearance of GP_{ex} dips at C_r is that in the tightly packed superlattices Laurdan's chromophore is squeezed more toward the phospholipid polar headgroup regions and consequently adopt a disposition more exposed to water, giving arise to a lower GP_{ex} than that in the less tightly packed irregular regions. At C_r, the area covered by regular distribution is maximal; therefore, Laurdan's GP_{ex} exhibits a minimum. A precedent example of Laurdan's chromophore being squeezed out more toward the polar headgroup regions is the case of Laurdan in the rigid and tightly packed bipolar tetraether archaeosomes.[32] Nevertheless, this explanation also uses the concepts proposed in the sterol regular distribution model.

Our observation of GP_{ex} dips at C_r is not contradictory to the results obtained by Parasassi et al.,[36] who reported that Laurdan's GP_{ex} in fluid dimyristoyl-L-α-phosphatidylcholine (DMPC) and dilauroyl-L-α-phosphatidylcholine (DLPC) MLVs exhibited GP_{ex} peaks at ~5, 15, 30, and 45 mol % cholesterol. In their study, large cholesterol increments (~5 mol %) were used, whereas our present study used much smaller cholesterol increments (0.3−0.4 mol %). When using large mole fraction increments, the actual cholesterol dependence of GP_{ex} could elude detection or the result may lead to an erroneous conclusion as illustrated in Figure 4B. The data in Figure 4B are taken from Figure 4A. When the data are plotted using the 11 mol % increment (top, Figure 4B), one could draw a wrong conclusion that Laurdan's GP_{ex} increases monotonically with increasing sterol content. When plotting the data using smaller sterol increments such as 3−5 mol % (middle and bottom, Figure 4B), multiple biphasic changes become somewhat observable and a local maximum in GP_{ex} at ~30 and 45 mol % cholesterol can be seen (bottom, Figure 4B), as reported by Parasassi et al.[36] However, 30 and 45 mol % are not the theoretically predicted C_r values, and the GP_{ex} peak/dip profile revealed in the bottom panel of Figure 4B is still not genuine compared to the data in Figure 4A. Thus, Figure 4, panels A and B, clearly demonstrates that the use of reasonably small sterol mole fraction increments (such as 0.3−0.4 mol %) over a wide range is necessary in order to correctly delineate the global as well as local effects of cholesterol content on membrane properties.

Comparison of Laurdan GP_{ex} Dips with DPH Polarization Peaks. To further demonstrate that the use of small cholesterol increments over a wide range is essential for detecting multiple biphasic changes in membrane properties at C_r, we conducted a similar study using DPH fluorescence polarization. DPH polarization reflects mainly the molecular order of lipid acyl chains. Using small cholesterol increments (0.3−0.4 mol %) over the range 18.3−28.0 mol %, we observed that DPH polarization displays an alternating variation with cholesterol content, exhibiting a distinct peak (termed as DPH polarization peaks) at 20.0, 22.0, 25.0, and 26.2 mol % cholesterol in cholesterol/POPC LUVs at 24 °C (Figure 5B). These mole fractions (Figure 5B) match well with the Laurdan's GP_{ex} dip positions (Figure 5A) in the same mole fraction region examined. Within the experimental errors, these DPH polarization peak positions (except for 26.2 mol %; Figure 5, panels A and B) agree with the theoretically predicted C_r values for maximal sterol superlattice formation. These results (Figure 5B) are consistent with our previous DPH polarization data obtained from cholesterol/DMPC MLVs.[25] It is important to note that, when the data from Figure 5B are replotted using larger cholesterol increments (e.g., 3 mol %, Figure 5C), the alternating variation of DPH polarization with cholesterol content may be completely eluded from detection (e.g., Figure 5C) and an erroneous conclusion for a linear change of DPH polarization with cholesterol content could be generated (e.g., Figure 5C). Our DPH polarization data (Figure 5, panels B and C) echo

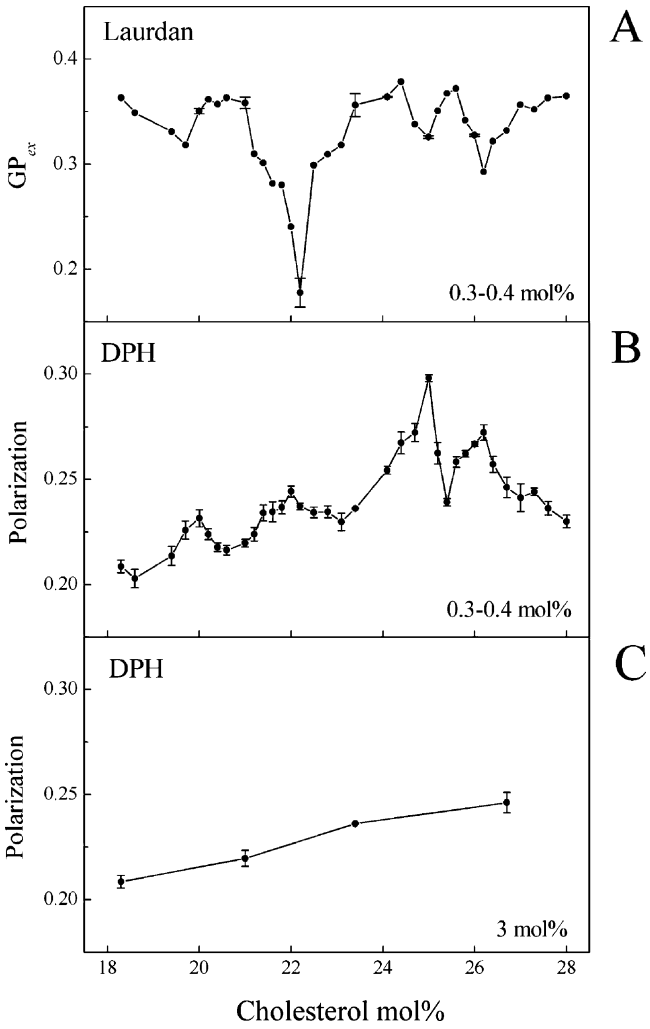

Figure 5. Comparison of (A) Laurdan's GP_{ex} and (B) DPH polarization as a function of cholesterol mol % in cholesterol/POPC LUVs. The data were obtained using 0.3−0.4 mol % increments. The data in panels A and B were obtained from the same vesicles under virtually the same thermal history. Temperature for measurements was 24 °C. The data in panel B are replotted in panel C using 3 mol % sterol increments.

that the use of small mole fraction increments over a wide range is necessary in order to delineate the genuine cholesterol effect on membrane properties.

There are prominent differences between DPH polarization peaks and Laurdan GP_{ex} dips. The DPH polarization peak at C_r = 22.2 mol % (Figure 5B) is shallow, whereas the Laurdan GP_{ex} dip at the same C_r (22.2 mol %) is quite pronounced (Figure 5A). At C_r = 25.0 mol %, DPH polarization exhibits a pronounced biphasic change (Figure 5B); in contrast, at the same C_r, Laurdan GP_{ex} displays only a shallow dip (Figure 5A). The C_r value 22.2 mol % is predicted by the centered rectangular superlattice model but not by the hexagonal superlattice model,[9,13,15] whereas the C_r value 25.0 mol % is predicted by the hexagonal superlattice model, not by the centered rectangular superlattice model (discussed in ref 13). It seems that Laurdan's GP_{ex} is more sensitive to the formation of centered rectangular superlattices whereas DPH polarization is more sensitive to the formation of hexagonal superlattices. The implication is that the lipid polar headgroup regions (reflected by the Laurdan GP_{ex}) undergo a more dramatic change in packing from a centered rectangular superlattice C_r (e.g., 22.2 mol %) to its neighboring non-C_r than from a hexagonal superlattice C_r (e.g., 25.0 mol %) to its neighboring non-C_r. This point helps to understand the dramatic change of GP_{ex} in the neighborhood of 40.0 mol % cholesterol (Figure 4A). Theoretically, 40.0 mol % can be a critical sterol mole fraction for either hexagonal or centered rectangular superlattice formation or both (discussed in ref 13). Since the GP_{ex} dip at C_r = 40.0 mol % is as deep as that at 22.2 mol % (Figure 4A), centered rectangular superlattice formation probably contributes very significantly to the GP_{ex} dip observed at 40.0 mol % (Figure 4A).

Another difference is that DPH polarization (Figure 5B) reaches a maximum at C_r whereas Laurdan's GP_{ex} (Figure 5A) reaches a minimum at C_r. As a rod-like molecule, DPH would fit well into a membrane lattice point without creating appreciable local packing perturbations. Thus, unlike Laurdan, DPH could reside in the regular regions. Laurdan is a probe for the glycerol backbone regions whereas DPH senses membrane order in the hydrophobic core. Because the regular regions are more tightly packed than the irregular regions and because the regularly distributed areas reach a maximum at C_r (Figure 1), DPH polarization displays a local maximum at C_r (Figure 5B and the data shown in ref 25). In contrast, Laurdan's GP_{ex} is sensitive to the water content (or the lipid polar groups) near the chromophore and exhibits a local minimum at C_r (Figure 4A) as a result of probe relocation due to changes in membrane lateral organization with cholesterol content, as discussed earlier.

All of the above-mentioned differences between DPH polarization and Laurdan GP_{ex} data suggest that the biphasic changes in membrane properties at C_r are detectable with both probes, when using small sterol mole fraction increments over a wide range. However, these two probes may sense different properties of sterol superlattices and exhibit different sensitivities to different types of superlattices.

B. Prevention from Sterol Oxidation. We have previously reported[9−11] that a sufficient vesicle incubation time is needed in order to observe multiple biphasic changes in membrane properties at C_r. Then, it is important to assess how cholesterol auto-oxidation incurred during vesicle incubation might affect superlattice formation. Compared to cholesterol, oxysterols (the oxidative products of cholesterol) have weaker interactions with neighboring phospholipid molecules due to the presence of additional polar groups on the sterol molecule.[37] The decreased

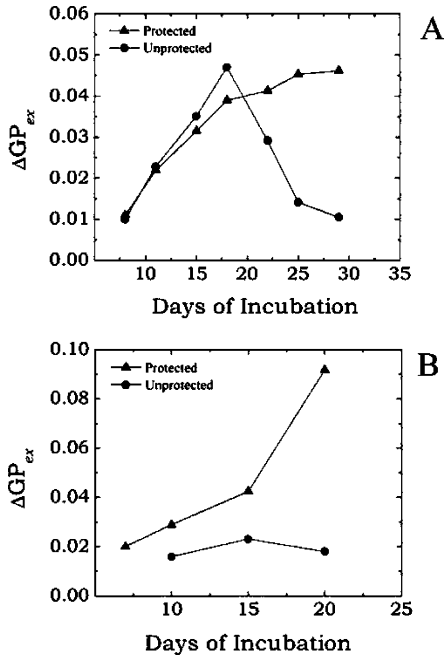

Figure 6. Effect of vesicle incubation time on the depth of the Laurdan's GP_{ex} dip (ΔGP_{ex}) detected at the critical sterol mole fraction (A) 50.0 mol % and (B) 33.3 mol % in cholesterol/POPC LUVs (diameter ∼160−180 nm) for two sets of samples: (dark triangles) protected and (dark circles) unprotected (not placed in the vacuum chamber nor flushed with argon) from sterol oxidation. Vesicles were incubated and GP_{ex} was measured at 24 °C. [POPC] = 40 μM.

interactions may attenuate superlattice formation. To test this possibility, we have investigated the cholesterol mole fraction dependence of Laurdan's GP_{ex} in two identical sets of testing samples: one being well protected from sterol oxidation during incubation using the method described in Materials and Methods and the other being prepared without full protection.

When the vesicles (near 50.0 mol % cholesterol in POPC) were well protected against sterol oxidation (dark triangles, Figure 6A), the depth of the GP_{ex} dip ($\Delta GP_{ex} = GP_{ex,max} - GP_{ex,min}$) exhibited a continuous increase over time and approached a steady state at ∼25−28 days. This result is reasonable because superlattices are self-assembled ordered structures. Their formation should increase over time, eventually reaching a maximum.

In sharp contrast, when the testing sample set in the neighborhood of 50.0 mol % cholesterol in POPC was not properly protected against sterol oxidation, the plot of ΔGP_{ex} vs incubation time exhibited a maximum at ∼18 days (Figure 6A, dark circles). Thereafter, ΔGP_{ex} decreased with time (Figure 6A, dark circles). The decrease of ΔGP_{ex} after ∼18 days may be attributed to sterol oxidation as demonstrated by the HPLC experiment (Figure 7). In this HPLC experiment, we extracted lipids (see Materials and Methods) from the same testing sample vesicles that were used in the GP_{ex} measurements and then used HPLC to analyze the extent of sterol oxidation in the lipid vesicles. The bottom panel in Figure 7 shows the HPLC elution profile of a sample extracted from 50.0 mol % cholesterol in POPC LUVs that were incubated for 25 days without full protection for sterol oxidation. In this elution profile, cholesterol and Laurdan (as an internal standard) were identified at the retention times of ∼1.0 and ∼2.5 min, respectively, whereas a sterol oxidation product appeared at ∼7.7 min. The top panel in Figure 7 is the elution profile obtained from the testing sample vesicles (also at 50.0 mol % cholesterol in POPC LUVs) that were well protected from sterol oxidation during the 25-day

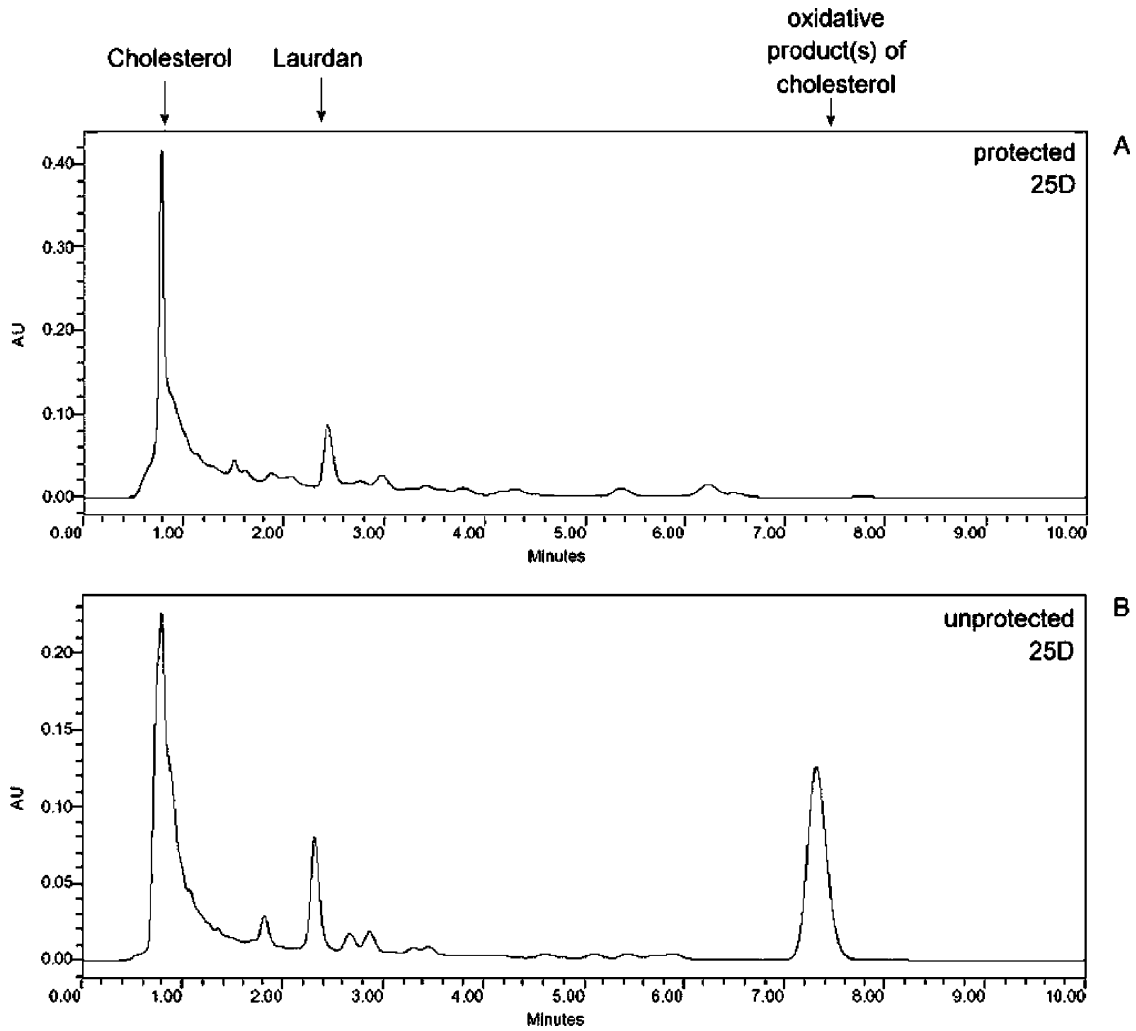

Figure 7. HPLC chromatograms of a sample extracted from LUVs (same as those used in Figure 6A) composed of 50 mol % cholesterol in POPC. (Bottom) The chromatogram obtained from vesicles unprotected from sterol oxidation; (Top) the elution profile from vesicles protected from sterol oxidation. The LUVs were incubated for 25 days at room temperature.

incubation period (using the procedures described in Materials and Methods). In this elution profile, cholesterol and Laurdan were detected at the expected retention times, but very little oxidized cholesterol was detected at ~7.7 min. These results support the idea that the oxidative product of cholesterol, which accumulates over time, attenuates sterol superlattice formation, therefore, leading to a decrease in ΔGP_{ex} after a certain time point (dark circles in Figure 6A).

A similar result was observed between the protected and unprotected cholesterol/POPC LUVs near the critical sterol mole fraction 33.3 mol % (Figure 6B). In this case, when the vesicles were well protected, ΔGP_{ex} increased with vesicle incubation time (dark triangles, Figure 6B). For the vesicles not well protected (dark circles, Figure 6B), the same sample set showed a very shallow GP_{ex} dip ($\Delta GP_{ex} = 0.01-0.02$), and ΔGP_{ex} did not increase over time.

The effect of sterol oxidation on ΔGP_{ex} can be calculated by using a kinetic model (see the Appendix). The calculation shows that the difference in the data obtained from the unprotected samples (dark circles) between panels A and B of Figure 6 may be due to the time difference for the beginning of sterol oxidation. When there is no sterol oxidation, the ΔGP_{ex} values calculated from the kinetic model can be fitted to the data experimentally obtained from the protected sample set (Figure 6A, triangles; see the Appendix).

Figures 6 and 7 together indicate that it is necessary to protect sterols from auto-oxidation in order to detect authentic multiple biphasic changes in membrane properties at C_r.

C. Consideration of Lipid Concentration, Vesicle Incubation Time, and the C_r Regions. Using small cholesterol mole fraction increments and the lipid vesicles that were well protected from oxidation, we have investigated the effects of lipid concentration and vesicle incubation time on the GP_{ex} dip. Figure 8A shows the evolution of the GP_{ex} dip profile over time for a set of cholesterol/POPC LUVs with [POPC] = 40 μM in the neighborhood of the critical sterol mole fraction 40 mol %. Before day 5 (D5, Figure 8A) of vesicle incubation, GP_{ex} does not show any significant dip in the sterol mole fraction range examined. On day 5 and thereafter, a GP_{ex} dip at 40.0 mol % becomes detectable, and the GP_{ex} dip becomes deeper over time (Figure 8A). Figure 8B shows a similar result obtained from cholesterol/POPC LUVs in another critical sterol mole fraction region (50.0 mol %) with [POPC] = 40 μM. Here [POPC] is referring to the phospholipid concentration in the testing samples.

The trend that the GP_{ex} dip becomes deeper over time can be quantitatively expressed in terms of the time dependence of ΔGP_{ex} as shown in Figure 8, panels C and D. For [POPC] = 40 μM (dark squares in Figure 8, panels C and D), ΔGP_{ex} at 40.0 and 50.0 mol % cholesterol increases with vesicle

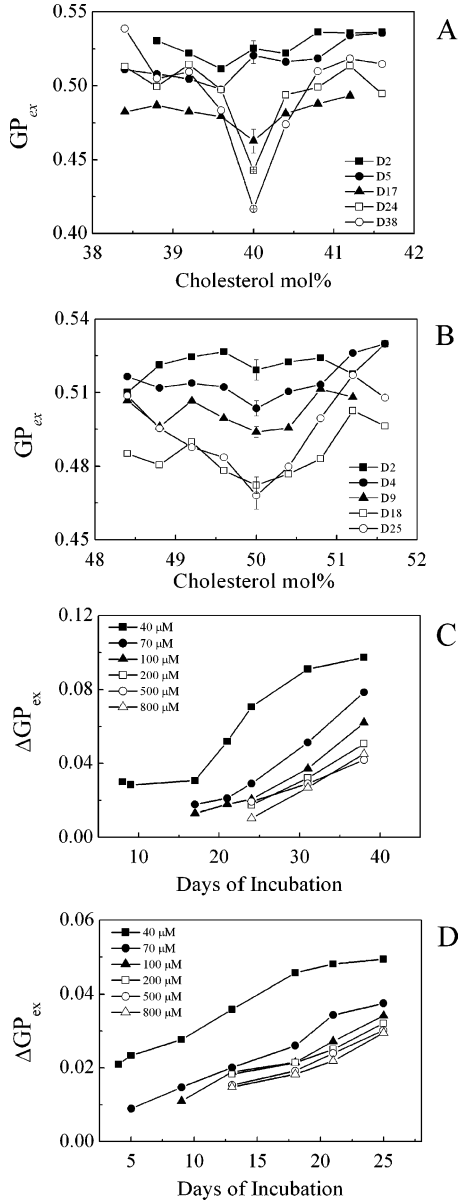

Figure 8. (A and B) Evolution of the GP_{ex} dip profile over time for a set of samples with [POPC] = 40 μM in the neighborhood of 40 and 50 mol % cholesterol in POPC LUVs, respectively. (C and D) Vesicle incubation time dependence of the depth of the GP_{ex} dip (ΔGP_{ex}) at different POPC concentrations in the testing sample set near 40 and 50 mol % cholesterol in POPC LUVs, respectively. Temperature = 24 °C.

incubation time and approaches a plateau after 38 and 25 days, respectively. This trend is in good agreement with the results shown in Figure 6 and consistent with the concepts proposed in the sterol superlattice model. Superlattices are self-assembled ordered lateral structures which take time to form. At the time of reaching the ΔGP_{ex} plateau, the membrane surface area covered by superlattices should reach a maximum.

The results from Figures 6 and 8 point out that sufficient vesicle incubation is needed in order to detect a biphasic change in membrane properties at C_r (as previously noticed).[9−11] When the lipid concentration of the testing sample vesicles is at 40 μM POPC, the minimal vesicle incubation time required for detection of a biphasic change at C_r at 33.3, 40.0, and 50.0 mol % is ∼3−5 days (triangles in Figure 6 and dark squares in Figure 8, panels C and D). During this incubation time period, vesicle size did not change significantly as determined by photon correlation spectroscopy (see Materials and Methods).

Figure 8, panels C and D, also shows that, as the POPC concentration in the testing samples increases, a longer vesicle incubation time is needed in order to detect the GP_{ex} dip at C_r = 40.0 and 50.0 mol % sterol. At a given incubation time, vesicles at a higher lipid concentration yield a lower ΔGP_{ex} (Figure 8, panels C and D). Another interesting observation is that, at high lipid concentrations (e.g., 100−800 μM), the minimal time required for the detection of the GP_{ex} dip varies with the C_r value, in contrast to the case of low [POPC] (e.g., 40 μM). For example, for [POPC] = 800 μM, the GP_{ex} dip at C_r = 40.0 mol % becomes detectable after 24 days incubation (Figure 8C), whereas the GP_{ex} dip at C_r = 50.0 mol % becomes detectable after 16 days incubation (Figure 8D). All of the data shown in Figure 8D were obtained from testing samples prepared from the same stock sample set. This stock sample set had a thermal history different from that used for the experiments shown in Figure 6A. This explains why the starting day for observing a GP_{ex} dip at C_r = 50.0 mol % in the 40 μM sample set shown in Figure 8D (dark squares) differs somewhat from that shown in Figure 6A (triangles).

Since ΔGP_{ex} reflects the extent of regularly distributed sterol superlattices, the data shown in Figure 8, panels C and D, may have revealed an important new concept for membrane cholesterol lateral organization. At high lipid concentrations, vesicle−vesicle interactions are increased so lipid mixing through collisions and coalescence is increased. In addition, at high lipid concentrations, the spontaneous transfer of lipids (including sterols and phospholipids) from donor vesicles to the aqueous phase and the subsequent reinsertion of lipids from the aqueous phase to acceptor vesicles become more frequent and more random. These would counteract superlattice formation, thus slowing down the formation of the GP_{ex} dips. This partially explains why some studies (e.g., nuclear magnetic resonance and differential scanning calorimetry) requiring high lipid concentrations may not detect biphasic changes in membrane properties at C_r[38] and why most evidence for sterol superlattices came from fluorescence studies which require much less lipids. If sufficient vesicle incubation time is given and other conditions described in this study are fulfilled, then multiple biphasic changes in membrane properties at C_r should be detectable for vesicle samples at high lipid concentrations (e.g., 800 μM to 5 mM) as shown in this study or as high as 45 mM in a recent pressure-perturbation calorimetry study (Chong, Zhao, Venegas, and Winter, unpublished data).

Figure 8, panels C and D, also suggest that the time and lipid concentration dependencies of the depth of the GP_{ex} dips (ΔGP_{ex}) may vary with C_r. This suggestion is reasonable because the geometric arrangement of lipids in superlattices varies with C_r and consequently the lattice constant within the superlattices also varies with C_r. In addition, since there is a difference in membrane packing between the regularly distributed superlattices and the irregular regions (Figure 1), the lattice constants in these two regions must differ too, and the differences will determine the size and shape of the interfacial area between the regular and irregular regions in a C_r dependent manner. Because of the changes in the lattice constant, the physical properties (e.g., lipid lateral diffusion, spontaneous inter-bilayer lipid transfer, and phospholipid polar headgroup conformation with respect to membrane surface) of superlattice-containing membranes are not the same at different C_r values.

With regard to lipid concentration dependence, the GP_{ex} dip at C_r = 22.2 mol % is rather unusual. The incubation time required for the detection of the GP_{ex} dip at C_r = 22.2 mol % (in the range of <3 days) does not change greatly with [POPC].

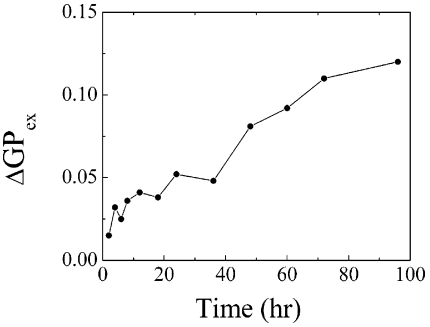

Figure 9. Effect of vesicle incubation time on the depth of the GP_{ex} dip (ΔGP_{ex}) detected at the critical sterol mole fraction 22.2 mol % for cholesterol/POPC LUVs with [POPC] = 40 μM.

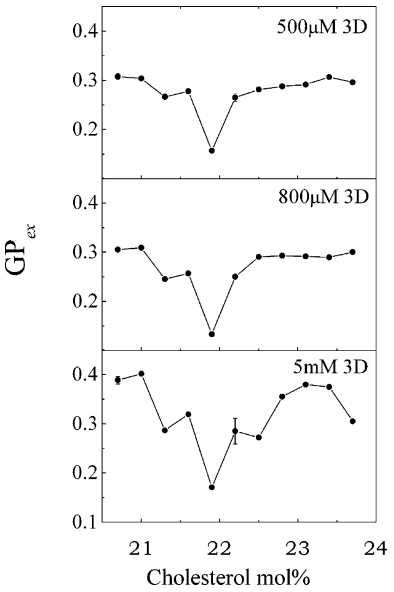

Figure 10. Plot of GP_{ex} versus cholesterol mole fraction in the neighborhood of 22.2 mol % in POPC LUVs at three different high POPC concentrations: 500, 800 and 5000 μM. Vesicle incubation time = 3 days.

At [POPC] = 40 μM, the GP_{ex} dip at C_r = 22.2 mol % cholesterol is detectable a few hours after vesicle formation, and the depth of the dip (ΔGP_{ex}) increases steadily over the time period of 4 days (Figure 9). At a much higher POPC concentration (e.g., 800 μM), the GP_{ex} dip at C_r = 22.2 mol % is still detectable on Day 3 (Figure 10, middle) similar to the case at [POPC] = 40 μM. In sharp contrast, at the same high POPC concentration (800 μM), the GP_{ex} dip at C_r = 50.0 and 40.0 mol % began to appear only after a long incubation such as 16 and 24 days, respectively (Figure 8). Also shown in Figure 10 is that the GP_{ex} dip at C_r = 22.2 mol % remained detectable also on day 3 despite that [POPC] was increased by 1 order of magnitude from 500 (Figure 10, top) to 5000 μM (Figure 10, bottom).

The insensitivity of ΔGP_{ex} at C_r = 22.2 mol % to lipid concentration (Figure 10) is rather unusual among all of the C_r regions examined; however, this insensitivity is possible according to the kinetic model presented in the Appendix. It is interesting to note that, in the sterol mole fraction range examined, 22.2 mol % is the only critical mole fraction predicted by the centered rectangular superlattice model[15] but not predicted by either the original hexagonal or extended hexagonal superlattice model.[13] At 22.2 mol %, the lipid acyl chains and the sterol molecules are arranged in a hexagonal matrix lattice where some sterol molecules are maximally separated into centered rectangular superlattices within the hexagonal matrix lattice. How this centered rectangular geometrical arrangement would create kinetic parameters (see the Appendix) different from those for hexagonal superlattice-containing membranes remains to be explored.

The GP_{ex} dip at C_r = 40.0 mol % is deep (Figure 4A) as is the dip at 22.2 mol %. However, the appearance of the GP_{ex} dip at 40.0 mol % is late (Figure 8), unlike the 22.2 mol % dip. This may be explained as follows. 40.0 mol % is a critical mole fraction for both centered rectangular and hexagonal superlattices. At this critical mole fraction, both types of superlattices may occur concurrently, which means two different lattice constants compete for regular regions. This competition may slow down the overall superlattice formation, delaying the appearance of the GP_{ex} dip at C_r = 40.0 mol % (Figure 8C). However, given a sufficient time, the centered rectangular superlattices at C_r = 40 mol % are finally generated, which contribute significantly to the pronounced GP_{ex} dip (as discussed earlier).

The finding that liposomes with a higher lipid concentration took a longer incubation time to display a biphasic change in Laurdan's GP_{ex} at most C_r values (Figure 8, panels C and D) and that a higher sterol mol % (40.0 mol % as compared to 22.2 mol %) did not facilitate the GP_{ex} dip formation argues against the idea that the biphasic changes in membrane properties at C_r are due to sterol-phospholipid complex formation. In fact, computer simulations of sterol superlattices[18] and the original sterol superlattice theories[9,15] do not require complex formation. However, the presence of multiple biphasic changes in membrane properties at C_r, or inferentially the presence of sterol superlattice, does not exclude the formation of sterol-phospholipid complex.[39] Complex formation and sterol superlattice may share the same physical origin and may just occur at different times. It is possible that sterol-phospholipid complexes are formed at the beginning of lipid membrane formation. Given a sufficient time, membrane lipids can move toward lateral equilibrium in the membrane, and subsequently, sterol superlattices are formed.

It is a misconception that because sterol superlattice formation in model membranes often requires long incubations (days), the superlattice is not existent in cell membranes. It is not appropriate to compare the time dependence of lateral organization in model membranes with that in biological membranes. Model membranes are prepared by perturbation methods such as vortexing, extrusion, sonication, electroformation, etc. from individual lipid molecules dissolved in organic solvents. For these model membranes, it takes time to reach lateral organization equilibrium or semiequilibrium after vesicle formation. In contrast, cell membranes are derived from their parent cells via much milder events (fission or cell division) in the absence of organic solvents. The basic framework of membrane lateral organization (e.g., lipid rafts) inherited from parent cell membranes should have been around for a long time, at least for the cell's lifetime ranging from days to years (e.g., ~45 years for human T cells), in spite of constant dynamic exchanges of membrane lipids due to lipid degradation and synthesis.

Summary

It can be summarized from this study and our previous studies[9−11,13,16,17,21−25,40] that, to detect multiple biphasic changes in membrane properties at C_r, one should (i) prevent sterols from oxidation, (ii) mix the lipid components thoroughly in organic solvent before vesicle formation, (iii) let vesicles subject to cooling and heating cycles and give sufficient incubation time, (iv) consider lipid concentrations, probe types, and C_r regions,

(v) use small sterol mole fraction increments (e.g., 0.3−0.4 mol %) over a wide sterol mole fraction range, (vi) determine the sterol mole fraction in each vesicle sample highly accurately, and (vii) keep all of the vesicles in the same sample set under the same thermal history prior to examination. This study suggests that not all of the sterol superlattices are the same and that the interfacial regions between the regularly distributed sterol superlattices and the irregular regions provide one of the primary mechanisms for biphasic changes in membrane properties (including enzyme and channel activities)[22,23,34,41] at C_r.

Acknowledgment. This work was supported by AHA (0255082N & 0655418U) and ACS-Petroleum Research Fund (PRF#38205-AC7). I.P.S. is grateful for the support of Mrs. Lawrence Garner, Dr. Diomedes Logothetis, Dr. Howard Brockman and Dr. Rhoderick Brown.

Appendix. Model of Superlattice Formation: Effects of Sterol Oxidation and Lipid Concentration

Structure of an Ordered Cluster of Cholesterol Molecules. Let us consider a cluster of ordered molecules (Figure 11). The ordered cluster contains both cholesterol and POPC molecules, and the cholesterol molecules form a superlattice. Because of thermal fluctuations, it may happen that there are small un-ordered islands inside an ordered cluster. These small un-ordered islands are not part of the host ordered cluster. Figure 11 shows only one small un-ordered island inside the large ordered cluster. The outer and inner peripheries of the large ordered cluster are also shown in Figure 11.

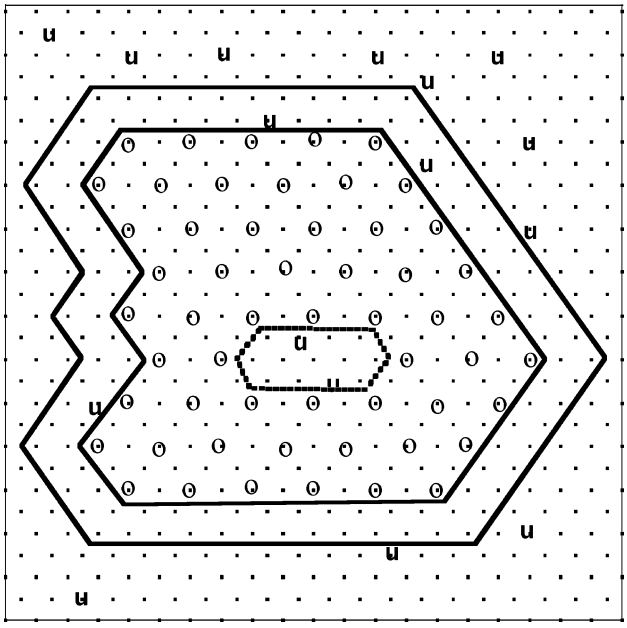

Figure 11. Configuration of an ordered cholesterol cluster. Small dots represent the hydrocarbon chains of POPC molecules, and open circles mark molecules of the ordered cholesterol cluster. The ordered cholesterol molecules form a superlattice. The outer periphery of the ordered cholesterol cluster is a stripe around the cluster marked by double solid line. The width of the stripe is the unit length of the superlattice. The un-ordered cholesterol molecules are marked by letters "u". There is one un-ordered inner island inside the ordered cholesterol cluster (surrounded by dotted lines). This inner island forms the inner periphery of the ordered cholesterol cluster.

Vesicle-Surrounding Interaction. There is lipid exchange between each vesicle and its surrounding. The exchange may take place by at least two mechanisms: (i) desorption and then transferred via the aqueous phase and (ii) vesicle−vesicle collision.[42] At high vesicle concentrations the lipid exchange arising from vesicle−vesicle collision dominates that due to desorption and aqueous-phase diffusion, according to Jones and Thompson.[42]

In order to give a quantitative description of the experimental results of this paper, the following simple kinetic model has been constructed.

Assumptions of the model are as follows:

(1) The total number of peripheral (outer + inner) molecules of the ordered clusters is proportional to the total number of molecules (cholesterol + POPC) forming the ordered clusters. This assumption for ordered clusters is true for compositional clusters (Sugar, unpublished results). The proportionality of cluster size vs cluster perimeter (outer + inner) was noticed when simulating gel-fluid clusters in DMPC/distearoyl-L-α-phosphatidylcholine bilayers. The results on cluster size vs outer perimeter were published in ref 43.

(2) During the equilibration process, the composition of each vesicle is assumed to be constant, i.e., fluctuates around a constant value. This fluctuation is the result of lipid exchange between the vesicle and its surrounding. The constant average composition can be maintained as follows: once a cholesterol (or POPC) molecule leaves the vesicle membrane the same or another cholesterol (or POPC) enters the membrane. These two events are coupled but they do not take place necessarily at the same place and at the same time. It is assumed, however, that the time scale of these coupled events is much shorter than the time scale of the equilibration. An essential assumption of our model is that the frequency of the lipid exchange increases and then levels off with increasing lipid concentration. The leveling off can be explained by an increasing number of vesicle aggregates. We have detected the aggregation of vesicles after about 5−8 days of incubation (unpublished result).

(3) Oxidized cholesterol cannot be in an ordered cluster of cholesterol molecules. If a cholesterol molecule of an ordered cluster is oxidized, it becomes part of the un-ordered region.

(4) The oxidation is a first-order chemical reaction, and the rate of oxidation is similar in the ordered and un-ordered phase.

(5) In our Laurdan experiments a GP_{ex} dip becomes detectable after 5−8 days of incubation. Thus, the experiments do not capture the nucleation phase of the formation of ordered cholesterol clusters. Because of this and to simplify our model, we do not consider the nucleation event.

In the model, every concentration is given in chain fraction, e.g., in the case of equimolar mixture of cholesterol and POPC the chain fraction is 0.333.

Let us consider an individual vesicle and use the following notations:

c_r, cholesterol concentration in the vesicle (it is the critical cholesterol concentration)

c_0^T, total concentration of cholesterol and POPC chains situated in ordered clusters

$c_0 = c_0^T c_r$, concentration of cholesterol situated in ordered clusters

$c_0^l = c_0^T(1 - c_r) = c_0(1 - c_r)/(c_r)$, concentration of POPC chains situated in ordered clusters

αc_0^T, total concentration of cholesterol and POPC chains situated at the periphery of the ordered clusters (see assumption 1)

αc_0, the concentration of cholesterol in the periphery if the ordered clusters were extended into the current peripheral region

c_u, concentration of cholesterol situated in un-ordered regions

$c_u^l = (c_r - c_0)(1 - c_r)/(c_r)$, concentration of POPC chains situated in un-ordered regions

c_u^T, total concentration of oxidized and un-oxidized cholesterol and POPC chains situated in un-ordered regions

c_u^{ox}, oxidized cholesterol concentration in un-ordered regions

N_c, average number of cholesterol in a vesicle

N_l, average number of POPC in a vesicle

$N_T = N_c + 2N_l$, average number of cholesterol plus POPC chains in a vesicle

The number of cholesterol (or chains) of certain properties can be obtained by multiplying the respective concentration by N_T. For example $N_T c_u^{ox}$ is the number of oxidized cholesterol in a vesicle.

c_l, total lipid concentration in the sample outside the considered vesicle (given in μM)

$f = 1 - \exp(-kc_l)$, the normalized frequency of the molecule exchange between the vesicle and its surrounding (see assumption 2). The frequency is normalized by the frequency at $c_l = \infty\ \mu M$.

The simple relationships between the above concentrations are

$$c_r = c_0 + c_u + c_u^{ox} \tag{1}$$

From assumption 4 follows that

$$c_0 + c_u = c_r e^{-k_{ox}t} \tag{2}$$

The change of c_0 during the equilibration can be described by the following differential equation

$$\frac{dc_o}{dt} = -k_{ox}c_o - k_{ou}c_o + k_{uo}\alpha c_o c_u - k_{oo}^e f c_o c_o^T - k_{oo}^{e'} f c_o^l c_o^T - k_{ou}^e f c_o c_u^T + k_{ou}^{ep} f\alpha c_o c_o - k_{ou}^{e'} f c_o^l c_u^T + k_{ou}^{ep'} f\alpha c_o c_o^l - k_{uo}^e f c_u c_o^T - k_{uo}^{e'} f c_u^l c_o^T - k_{uo}^{e''} f c_u^{ox} c_o^T + k_{uu}^{ep} f\alpha c_o c_u + k_{uu}^{ep'} f\alpha c_o c_u^l \tag{3}$$

On the right-hand side of eq 3, the meaning of the terms is as follows:

$-k_{ox}c_o$, oxidation of ordered phase cholesterol (oxidation of ordered cholesterol always results in local disorder; see assumption 3)

Cholesterol−POPC Chain Exchanges through Intramembrane Diffusion.

$-k_{ou}c_o$, exchanging an ordered cholesterol with a nearest neighbor POPC chain. This change transforms ordered cholesterol into an un-ordered one. For the experimental cholesterol/POPC mole fractions in the ordered phase, each cholesterol molecule is surrounded only by POPC chains. Thus, the number of possible cholesterol/POPC exchange is proportional to c_o.

$+k_{uo}\alpha c_o c_u$, increasing ordered region in the periphery by local cholesterol−POPC chain exchange. These changes transform un-ordered cholesterol into an ordered one. The rate of these changes is proportional to the size of the periphery and to the number of un-ordered cholesterol molecules.

Cholesterol and POPC Translocations through Membrane−Surrounding Interactions.

Translocation refers to the pair of events: a molecule leaves the vesicle membrane and, shortly after this, a similar type of molecule enters the membrane. This pair of events maintain a constant average vesicle composition (see assumption 2). The rate of any translocation is proportional to the product of two probabilities: the probability that a molecule leaves the membrane and the probability that a similar molecule enters the membrane. As an example, let us consider cholesterol translocation from the un-ordered to the ordered phase. The probability that a cholesterol from the un-ordered phase leaves the vesicle membrane is proportional to the number of cholesterols in that phase, c_u. The probability that a cholesterol enters from the aqueous surrounding to the ordered phase of the vesicle membrane is proportional to the size of the ordered phase, c_o^T. Thus the rate of cholesterol translocation from the un-ordered to the ordered phase is $-k_{uo}^e f c_u c_o^T$ where f is the normalized overall frequency of the translocation events between the vesicle and its surrounding. This frequency depends on the lipid concentration of the sample (see assumption 2). The negative sign signifies that this particular translocation decreases the ordered phase. Note that inserting an extra cholesterol into the ordered phase would result in local disorder. k_{uo}^e is the rate constant of the particular translocation event. Below we list the rates of the translocations that affect the amount of ordered cholesterol molecules.

$-k_{oo}^e f c_o c_o^{T,}$ cholesterol translocation within the ordered phase

$-k_{oo}^{e'} f c_o^l c_o^T$, POPC translocation within the ordered phase

$-k_{ou}^e f c_o c_u^T + k_{ou}^{ep} f c_o \alpha c_o$, cholesterol translocation from ordered to un-ordered phase. The second term refers to translocation creating ordered region in the periphery.

$-k_{ou}^{e'} f c_o^l c_u^T + k_{ou}^{ep'} f\alpha c_o c_o^l$, POPC translocation from ordered to un-ordered phase. The second term refers to translocation creating an ordered region in the periphery.

$-k_{uo}^e f c_u c_o^T$, cholesterol translocation from the un-ordered to the ordered phase

$-k_{uo}^{e'} f c_u^l c_o^T$, POPC translocation from the un-ordered to the ordered phase

$-k_{uo}^{e''} f c_u^{ox} c_o^T$, oxidized cholesterol translocation from the un-ordered to the ordered phase

$+k_{uu}^{ep} f c_u \alpha c_o$, cholesterol translocation from an un-ordered phase to the periphery of the ordered phase. The translocation creates an ordered region in the periphery.

$+k_{uu}^{ep'} f c_u^l \alpha c_o$, POPC translocation from an un-ordered phase to the periphery of the ordered phase. The translocation creates an ordered region in the periphery.

After substituting eq 2 into eq 3 and converting concentrations to c_o, we obtain

$$\frac{dc_0}{dt} = -(C - Df)c_o^2 + (A + A_o e^{-k_{ox}t} - [B + B_o e^{-k_{ox}t}]f)c_o \tag{4}$$

where

$$A_o = k_{uo}\alpha c_r, \quad A = -k_{ou} - k_{ox}$$

$$-B_o = -k_{uo}^e + k_{uu}^{ep}\alpha c_r + k_{uo}^{e''}$$

$$-B = -k_{ou}^e - k_{ou}^{e'}\frac{1 - c_r}{c_r} - k_{uo}^{e'}\frac{1 - c_r}{c_r} - k_{uo}^{e''} + k_{uu}^{ep'}\alpha(1 - c_r)$$

$$C = k_{uo}\alpha$$

$$D = \frac{1}{c_r}(-k_{oo}^e + k_{ou}^e + k_{uo}^e) + \frac{1 - c_r}{c_r c_r}(-k_{oo}^{e'} + k_{ou}^{e'} + k_{uo}^{e'} + k_{ou}^{ep'}\alpha c_r - k_{uu}^{ep'}\alpha c_r) + k_{ou}^{ep}\alpha - k_{uu}^{ep}\alpha$$

One can transform this nonlinear, first order, ordinary differential equation into a linear, inhomogeneous first order, ordinary differential equation by the following substitution:

$$c_0(t) = 1/z(t) \quad (5)$$

and we obtain

$$\frac{dz}{dt} = (C - Df) - (A + A_o e^{-k_{ox}t} - [B + B_o e^{-k_{ox}t}]f)z \quad (6)$$

The solution of eq 6 is

$$\frac{1}{c_0(t)} = z(t) = \exp\{-\int_{t_0}^{t}(A + A_o e^{-k_{ox}t'} - [B + B_o e^{-k_{ox}t'}]f)\,dt'\}|(C - Df)\int_{t_0}^{t}\exp\{\int_{t_0}^{t'}(A + A_o e^{-k_{ox}t''} - [B + B_o e^{-k_{ox}t''}]f)\,dt''\}\,dt' + z(t_0)| = \exp\left\{-(A - Bf)(t - t_0) + \frac{A_o - B_o f}{k_{ox}}(e^{-k_{ox}t} - e^{-k_{ox}t_0})\right\} \times \left[z(t_0) + (C - Df)\int_{t_0}^{t}\exp\left\{(A - Bf)(t' - t_0) - \frac{A_o - B_o f}{k_{ox}}(e^{-k_{ox}t'} - e^{-k_{ox}t_0})\right\}dt'\right] \quad (7)$$

In general the integral in eq 7 can only be numerically integrated. Calculating the integral, we use the method of Gaussian Quadratures.[44] However, when there is no oxidation, i.e. $k_{ox} = 0$, one can calculate the integral and get

$$\frac{1}{c_0(t)} = z(t) = z(t_0)\exp\{-(A + A_o - [B + B_o]f)(t - t_0)\} + \frac{C - Df}{A + A_o - [B + B_o]f}[1 - \exp\{-(A + A_o - [B + B_o]f)(t - t_0)\}] \quad (8)$$

In order to make a comparison between the experimental data and our model, we assume that the measured ΔGP_{ex} is proportional with c_o, the concentration of cholesterol molecules situated in the ordered phase, where the proportionality constant is marked by $\gamma (= \Delta GP_{ex}/c_o)$.

Equation 8 can be fitted to the data given in Figure 6a (triangles; for samples protected from oxidation). The parameters of eq 8 can be obtained from the experimental conditions ($c_r = 0.33$ and $c_l \cong 40\ \mu$M) and from the experimental data (ΔGP_{ex}-($t_o = 8$ days) $= \gamma c_o(t_o) = 0.011$). The remaining two parameters, $A + A_o - [B + B_o]f = 0.2967 \pm 0.0218$ day^{-1} and $\Delta GP_{ex}(\infty) = 0.04547 \pm 0.0011 (= \gamma c_0\,(\infty) = \gamma(A + A_o - [B + B_o]f)/(C - Df))$ were obtained by fitting eq 8 to the experimental data (solid lines, Figures 12 and 13).

Equation 8 can also be used to calculate the equilibration in the case of different lipid concentrations, c_l. In order to do this, the following parameter values have to be specified: $A + A_o$, $B + B_o$, C, D, and k. There are two relationships between these parameters

$$\Delta GP_{ex}(t = \infty, c_l = 40\ \mu\text{M}) = 0.04547 = \frac{A + A_o - [B + B_o](1 - \exp[-kc_l])}{C - D(1 - \exp[-kc_l])} \quad (9)$$

and

$$0.2967 = A + A_o - [B + B_o](1 - \exp[-kc_l]) \quad (10)$$

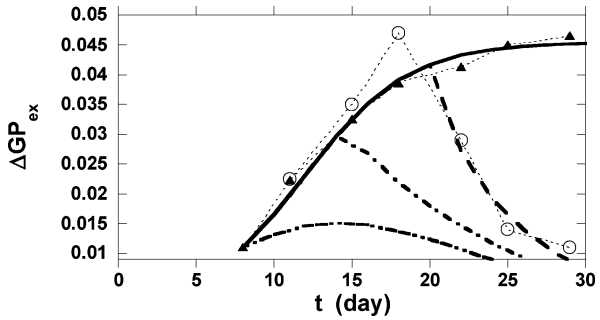

Figure 12. Calculated equilibration curves showing the effects of oxidation on ΔGP_{ex}. Solid line: equilibration curve calculated by using eq 8. System is protected from oxidation, i.e., $k_{ox} = 0$ day^{-1}. Respective experimental data from Figure 6a are marked by triangles. Dashed line: from day 8−20 time interval the equilibration curve has been calculated by using eq 8 (system is protected from oxidation, i.e., $k_{ox} = 0$ day^{-1}), whereas after day 20, eq 7 has been used (system is unprotected from oxidation, $k_{ox} = 0.0009$ day^{-1}). Open circles mark the respective experimental data from Figure 6a. In the case of dash-dotted and double dash-dotted line the system becomes un-protected from days 15 and 8, respectively. The parameters of eq 7 and eq 8 are as follows: $A - Bf = -15.326715 - k_{ox} + 0.90928 \cdot B_o$ day^{-1}; $A_o - B_o f = 15.623423 - 0.90928 \cdot B_o$ day^{-1}; $B_o = 0$ day^{-1}; $C - Df = 6.52523$ day^{-1}; $c_l = 40\ \mu$M.

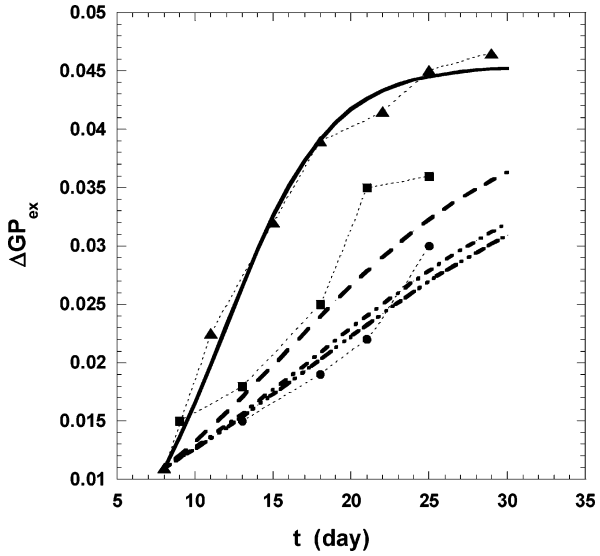

Figure 13. Calculated equilibration curves showing the effects of lipid concentration. Equilibration curves calculated by using eq 8 (system is protected from oxidation, i.e., $k_{ox} = 0$ day^{-1}) at the following lipid concentrations, c_l: 40 (solid line), 70 (dashed line), 100 (dash-dotted line), and 200 μM (double dash-dotted line). The parameters of eq 8 are as follows: $k = 0.06\ \mu\text{M}^{-1}$; $A + A_o = 2.26826$ day^{-1}; $B + B_o = 2.16826$ day^{-1}; $C = 46.8703$ day^{-1}, and $D = 44.3703$ day^{-1}. Triangles (40 μM POPC), squares (70 μM), and circles (100 and 200 μM) are the corresponding experimental data from Figures 6A and 8D.

In order to generate two other relationships, based on the trend of the experimental data, we assume that

$$\Delta GP_{ex}(t = \infty, c_l = 0\ \mu\text{M}) = 0.04839 = \frac{A + A_o}{C}$$

$$\Delta GP_{ex}(t = \infty, c_l = \infty\ \mu\text{M}) = 0.04 = \frac{A + A_o - [B + B_o]}{C - D}$$

By using these four relationships, one can eliminate $A + A_o$, $B + B_o$, C, and D from eq 8, and k remains the only parameter value to be determined. After fitting eq 8 to the experimental equilibration curve, taken at $c_l = 70\ \mu$M (closed circles, Figure

8d), we get $k = 0.06\ \mu M^{-1}$. After determining k, we can solve the above four algebraic equations and get the remaining parameter values: $A + A_o = 2.26826\ day^{-1}$, $B + B_o = 2.16826\ day^{-1}$, $C = 46.8703\ day^{-1}$, and $D = 44.3703\ day^{-1}$.

By using these parameter values in eq 8, the equilibration has been calculated for four different lipid concentrations, $c_l = 40$, 70, 100, and 200 μM (Figure 13). The calculated curves are in quite good agreement with the experimental equilibration curves. Note that in order to achieve this agreement it was necessary to assume lipid exchange with the surrounding and that the normalized frequency of the lipid exchange $f = 1 - \exp[-kc_l]$ increases with increasing lipid concentration. The exchange frequency increases by only 10% while the lipid concentration increases from 40 μM to infinity.

In most experiments with increasing lipid concentration, c_l, the equilibrium depth of a dip $\Delta GP_{ex}(t = \infty)$ decreases and then levels off. However, in the case of 0.222 cholesterol/POPC mole fraction $\Delta GP_{ex}(t = \infty)$ does not change with c_l (Figure 10). According to our model $\Delta GP_{ex}(t = \infty)$ does not practically depend on the lipid concentration when $A + A_o \gg B + B_o$ and$C \gg D$.

Let us consider now a case when the sample is protected from oxidation up to a certain time, t_{ox} and then it is unprotected. One can calculate the equilibration process from t_o to t_{ox} as before by using eq 8, but for $t_{ox} < t$, one has to use the more general formula given by eq 7. In eq 7, there is one additional model parameter, k_{ox}, the rate of cholesterol oxidation, and we also have to know the values of $A - Bf$ and $A_o - B_of$.

The available relationships are as follows: $C = k_{uo}\alpha$, $A_o = k_{uo}\alpha c_r$, $A = -k_{ou} - k_{ox}$, $B + B_o = 2.16826\ day^{-1}$, $C = 46.8703\ day^{-1}$. If $k_{ox} = 0$ $A + A_o = -k_{ou} + A_o = 2.26826\ day^{-1}$ and if $c_l = 40\ \mu M$, $f = (1 - \exp[-kc_l]) = 0.90928$. By using these relationships, we get $A_o = Cc_r = 46.87027 \times 0.333 = 15.623423\ day^{-1}$, $k_{ou} = 13.35516\ day^{-1}$, $A = -13.35516 - k_{ox}$, $B = 2.16826 - B_o$, and finally, $A - Bf = -15.326715 - k_{ox} + 0.90928 \cdot B_o$ and $A_o - B_of = 15.623423 - 0.90928 \cdot B_o$. Thus, eq 7 can be calculated by specifying the values of B_o and k_{ox}.

By using our model, we would like to calculate the experimental data presented in Figure 6a (circles). According to these experimental data, the oxidation started at $t_{ox} \approx 20$ days. A good fit was obtained between the experimental and calculated data at the following parameter values: $B_o = 0\ day^{-1}$ and $k_{ox} = 0.0009\ day^{-1}$ (bold dashed line and open circles, Figure 12). Note that the result is only slightly sensitive to the value of B_o. By using the same model parameter values, we calculated the equilibration curve at two other t_{ox} values: 15 and 8 days (see dash-dotted and double dash-dotted line, respectively, in Figure 12). The experimental results in Figure 6b for unprotected systems are qualitatively similar to the calculated double dash-dotted line in Figure 12. Based on this similarity, we think the sealing of the sample tubes was damaged early in these experiments.

Abbreviations

C_r, critical sterol mole fractions for maximal superlattice formation

DLPC, dilauroyl-L-α-phosphatidylcholine

DMPC, dimyristoyl-L-α-phosphatidylcholine

DPH, 1,6-diphenyl-1,3,5-hexatriene.

GP_{ex}, excitation generalized polarization

ΔGP_{ex}, depth of the GP_{ex} dip

Laurdan, 6-lauroyl-2-(dimethylamino)naphthalene

LUV, large unilamellar vesicles

MLV, multilamellar vesicles

POPC, 1-palmitoyl-2-oleoyl-L-α-phosphatidylcholine

References and Notes

(1) Pike, L. J.; Han, X.; Gross, R. W. *J. Biol. Chem.* **2005**, *280*, 26796−26804.

(2) Xu, W.; Yoon, S.-I.; Huang, P.; Wang, Y.; Chen, C.; Chong, P. L.-G.; Liu-Chen, L.-Y. *J. Pharm. Expt. Thera.* **2006**, *317*, 1295−1306.

(3) Gaus, K.; Gratton, E.; Kable, E. P.; Jones, A. S.; Gelissen, I.; Kritharides, L.; Jessup, W. *Proc. Natl. Acad. Sci. U.S.A.* **2003**, *100*, 15554−15559.

(4) Hartel, S.; Fanani, M. L.; Maggio, B. *Biophys. J.* **2005**, *88*, 287−304.

(5) Sot, J.; Bagatolli, L. A.; Goñi, F. M.; Alonso, A. *Biophys. J.* **2006**, *90*, 903−914.

(6) Nicolini, C.; Baranski, J.; Schlummer, S.; Palomo, J.; Burgues, M. L.; Kahms, M.; Kuhlmann, J.; Sanchez, S.; Gratton, E.; Waldmann, H.; Winter, R. *J. Am. Chem. Soc.* **2006**, *128*, 192−201.

(7) Simons, K.; Ikonen, E. *Nature* **1997**, *387*, 569−572.

(8) Kusumi, A.; Koyama-Honda, I.; Suzuki, K. *Traffic* **2004**, *5*, 213−230.

(9) Chong, P. L.-G. *Proc. Natl. Acad. Sci. U.S.A.* **1994**, *91*, 10069−10073.

(10) Chong, P. L.-G.; Olsher, M. *Soft Mater.* **2004**, *2*, 85−108.

(11) Chong, P. L.-G.; Sugar, I. P. *Chem. Phys. Lipids.* **2002**, *116*, 153−175.

(12) Somerharju, P.; Virtanen, J. A.; Cheng, K. H. *Biochim. Biophys. Acta.* **1999**, *1440*, 32−48.

(13) Liu, F.; Sugar, I. P.; Chong, P. L.-G. *Biophys. J.* **1997**, *72*, 2243−2254.

(14) Virtanen, J. A.; Somerharju, P.; Kinnunen, P. K. J. *J. Mol. Electron.* **1988**, *4*, 233−236.

(15) Virtanen, J. A.; Ruonala, M.; Vauhkonen, M.; Somerharju, P. *Biochemistry* **1995**, *34*, 11568−11581.

(16) Tang, D.; Chong, P. L.-G. *Biophys. J.* **1992**, *63*, 903−910.

(17) Chong, P. L.-G.; Tang, D.; Sugar, I. P. *Biophys. J.* **1994**, *66*, 2029−2038.

(18) Huang, J. *Biophys. J.* **2002**, *83*, 1014−1025.

(19) Huang, J.; Feigenson, G. W. *Biophys. J.* **1999**, *76*, 2142−2157.

(20) Parker, A.; Miles, K.; Cheng, K. H.; Huang, J. *Biophys. J.* **2004**, *86*, 1532−1544.

(21) Wang, M. M.; Sugar, I. P.; Chong, P. L.-G. *Biochemistry* **1998**, *37*, 11797−11805.

(22) Wang, M. M.; Olsher, M.; Sugar, I. P.; Chong, P. L.-G. *Biochemistry* **2004**, *43*, 2159−2166.

(23) Liu, F.; Chong, P. L.-G. *Biochemistry* **1999**, *38*, 3867−3873.

(24) Olsher, M.; Yoon, S.-I.; Chong, P. L.-G. *Biochemistry* **2005**, *44*, 2080−2087.

(25) Chong, P. L.-G.; Liu, F.; Wang, M. M.; Truong, K.; Sugar, I. P.; Brown, R. E. *J. Fluoresc.* **1996**, *6*, 221−230.

(26) Bartlett, G. R. *J. Biol. Chem.* **1959**, *234*, 466−468.

(27) Parasassi, T.; De Stasio, G.; Ravagnan, G.; Rusch, R. M.; Gratton, E. *Biophys. J.* **1991**, *60*, 179−189.

(28) Chong, P. L.-G.; Wong, P. T. T. *Biochim. Biophys. Acta.* **1993**, *1149*, 260−266.

(29) Bagatolli, L. A.; Gratton, E. *Biophys. J.* **1999**, *77*, 2090−2101.

(30) Bagatolli, L. A.; Gratton, E. *Biophys. J.* **2000**, *78*, 290−305.

(31) Parasassi, T. G.; Krasnowska, E.; Bagatolli, L. A. *J. Fluoresc.* **1998**, *8*, 365−373.

(32) Bagatolli, L. A.; Gratton, E.; Khan, T. K.; Chong, P. L.-G. *Biophys. J.* **2000**, *79*, 416−425.

(33) Fidorra, M.; Duelund, L.; Leidy, C.; Simonsen, A. C.; Bagatolli, L. A. *Biophys. J.* **2006**, *90*, 4437−4451.

(34) Helrich, C. S.; Schmucker, J. A.; Woodbury, D. J. *Biophys. J.* **2006**, *91*, 1116−1127.

(35) Parasassi, T. G.; Gratton, E. *J. Fluoresc.* **1995**, *5*, 59−69.

(36) Parasassi, T. G.; Giusti, A. M.; Raimondi, M.; Gratton, E. *Biophys. J.* **1995**, *68*, 1895−1902.

(37) Moore, N. F.; Patzer, E. J.; Barenholz, Y.; Wagner, R. R. *Biochemistry* **1997**, *16*, 4708−4715.

(38) de Almeida, R. F.; Fedorov, A.; Prieto, M. *Biophys. J.* **2003**, *85*, 2406−2416.

(39) Radhakrishnan, A.; McConnell, H. M. *Biophys. J.* **1999**, *77*, 1507−1517.

(40) Wang, M. M.; Sugar, I. P.; Chong, P. L.-G. *J. Phys Chem. B* **2002**, *106*, 6338−6345.

(41) Cuevas, F. J.; Jameson, D. M.; Sotomayor, C. P. *Biochemistry* **2006**, *45*, 13855−13868.

(42) Jones, J. D.; Thompson, T. E. *Biochemistry* **1989**, *28*, 129−134.

(43) Sugar, I. P.; Michonova-Alexova, E.; Chong, P. L.-G. *Biophys. J.* **2001**, *81*, 2425−2441.

(44) Press, W. H.; Flannery, B. P.; Teukolsky, S. A. In *Numerical Recipes*; Cambridge University Press: New York, 1989; Chapter 4.5, pp 121−126.